www.czasopisma.pan.pl PAN www.journals.pan.pl
ARCHIVES OF ACOUSTICS Vol. 47, No. 2, pp. 213–221 (2022), doi: 10.24425/aoa.2022.141651

Research Paper

A Honeycomb Based Graded Metamaterial Muffler with Broadband Sound Attenuation and Load Bearing Performances

Gen LI(1),(2), Yan CHEN(1),(2), Huan HE(1),(2),(3),(4)*

(1) *State Key Laboratory of Mechanics and Control of Mechanical Structures*
Nanjing University of Aeronautics and Astronautics
Nanjing 210016, China

(2) *Institute of Vibration Engineering Research*
Nanjing University of Aeronautics and Astronautics
Nanjing 210016, China

(3) *MIIT Key Laboratory of Multi-Functional Lightweight Materials and Structures*
Nanjing 210016, China

(4) *Laboratory of Aerospace Entry, Descent and Landing Technology*
Beijing 100094, China
*Corresponding Author e-mail: hehuan@nuaa.edu.cn

(*received November 19, 2021; accepted March 12, 2022*)

A challenge for developing acoustic metamaterials (AMMs) is considering the application of broadband muffling and load bearing capacity simultaneously. In this paper, a honeycomb based graded AMM muffler is proposed, which can widen the attenuation band and improve the structural stiffness without any external device by means of integrated design. Firstly, the acoustic and mechanical characteristics of the muffler unit cell are theoretically and numerically studied, and the graded muffler is designed based on these characteristics. The numerical results show that the graded muffler widens the attenuation bandwidth of the unit cell, and the simulation also shows that the graded muffler has greater stiffness than the uniform one. The stiffness driven muffler provides new possibilities for the design of advanced metamaterial with simultaneous sound insulation and load bearing performances.

Keywords: acoustic metamaterials; honeycomb structure; phononic crystal; local resonance.

1. Introduction

In recent years, phononic crystals (PCs) or acoustic metamaterials (AMMs) have attracted extensive attention due to their unusual ability to manipulate elastic waves and flexible design (DEYMIER, 2013). By introducing the concept of phonon band gap (NARAYANAMURTI *et al.*, 1979; SIGALAS, ECONOMOU, 1992; KUSHWAHA *et al.*, 1993), the sound insulation effect of AMMs can be explained from the perspective of wave mechanics. Band gaps represent frequency ranges where waves cannot pass through. Initially, the generation of band gaps is thought to be attributed to the destructive interference in a periodic structure (MARTÍNEZ-SALA *et al.*, 1995; MONTERO DE ESPINOSA *et al.*, 1998; VASSEUR *et al.*, 1998; SHAO *et al.*, 2020; CHEN *et al.*, 2021a; 2021b), so the lattice constant must be of the same scale as the wavelength. Later, due to the low frequency band gaps induced by local resonances (LIU *et al.*, 2000), it is possible for AMMs to control elastic waves by elaborately designed subwavelength scale microstructure (QIAN, SHI, 2017), which provides a new solution for low frequency noise reduction. However, the development of AMMs is still restricted by the narrow band gap width and the sensitivity to external load. Many scholars have made impressive contributions to solving these problems by using external devices such as absorbers, circuits, and

magnetic fields (Brennan, 1997; Nishida, Koopmann, 2007; Wang *et al.*, 2011; Popa *et al.*, 2013; Chen *et al.*, 2014; Wang, Chen, 2015; Xiao *et al.*, 2015). In spite of this, it is still challenging to achieve the integrated design of AMMs with broadband sound attenuation and load bearing performances.

Cellular honeycomb structures appear widely in nature and are manufactured on a large scale (Wang, 2019). In the past two decades, a large number of studies has been conducted on the basic mechanical behaviour of honeycomb structures (Camata, Shing, 2010; Asprone *et al.*, 2013; Sun *et al.*, 2017; Li *et al.*, 2018). When honeycomb structures are subjected to out-of-plane compression loads, their stiffness is almost the same as that of solid materials with the same thickness (Fan *et al.*, 2006; Khan *et al.*, 2012). To satisfy the various requirements with the development of scientific engineering, many creative honeycomb based structures are proposed (Michailidis *et al.*, 2009; Correa *et al.*, 2015; Chen *et al.*, 2016; Han *et al.*, 2016; Huang *et al.*, 2016; Wang *et al.*, 2021). By embedding the honeycomb cells with different materials or structures, such as foam, tubes, or even other polymer materials, honeycombs can be designed to have desirable properties (Zarei Mahmoudabadi, Sadighi, 2011; Xiang, Du, 2017; Liu *et al.*, 2018; Wang, Liu, 2018, 2019).

Functionally graded materials (FGMs) are advanced engineering materials designed for a specific performance or function in which a spatial gradation in structure and/or composition lend themselves to tailored properties (Naebe, Shirvanimoghaddam, 2016). Originally, FGMs are designed to relax the internal thermal stress by gradually changing their composition from metallic to ceramic (Kawasaki, Watanabe, 1997). Nowadays, FGMs have extended their applications to electronics, chemistry, optic, biomedicine, nuclear engineering, civil engineering, and many other fields (Koizumi, 1997). A large number of studies has been conducted on the special properties of FGMs (Aboudi *et al.*, 1999; Cheng, 2001; Shen, 2002; Chen, Lee, 2003; Tsukamoto, 2003; Jabbari, Sohrabpour, 2014). In brief, the superior performances of FGMs come from the spatially inhomogeneous composition or microstructure.

In this paper, a honeycomb based graded metamaterial muffler is proposed. By embedding the honeycomb cells with local resonance microstructures, the requirements of noise reduction and bearing capacity can be simultaneously satisfied. As a kind of stiffness driven honeycomb structure, it can be designed to meet the deformation requirements. Acoustically, the honeycomb frame can satisfy the general broadband sound insulation, while the local resonance microstructures are used to attenuate the strong noise in the specific frequency band. The band gap broadening can be realised by the combination of multiple unit cells with lattice constant graded variation. First, we study the muffler unit cell (Fig. 1a) and obtain the relationship between lattice constant and its acoustic and mechanical properties. Then we combine unit cells of different sizes into a graded muffler (Fig. 1b) to widen the band gap. The out-of-plane load bearing capacity of different configurations is also tested numerically. The results show that both the acoustic and mechanical properties of the graded muffler are better than those of the uniform one. Different from conventional acoustic metamaterial, due to the structural and functional integration design, this muffler does not require an external device to adjust the band gap, which means that it has higher reliability and robustness. Compared with membrane type or traditional plate type AMMs, this honeycomb based muffler is more resistant to out-of-plane deformation. In contrast to AMMs relying on soft materials such as rubber, the acoustic band gap of this muffler is independent of the structural material, so different materials can be selected according to the amplitude of the load. Since it is made of single material, it can be conveniently fabricated by additive manufacturing technology, leading to a broad application prospect. For instance, periodic graded mufflers (Fig. 1c) can be used as a sound insulation floor of an aircraft cabin (Fig. 1d) thus providing a quieter environment for passengers.

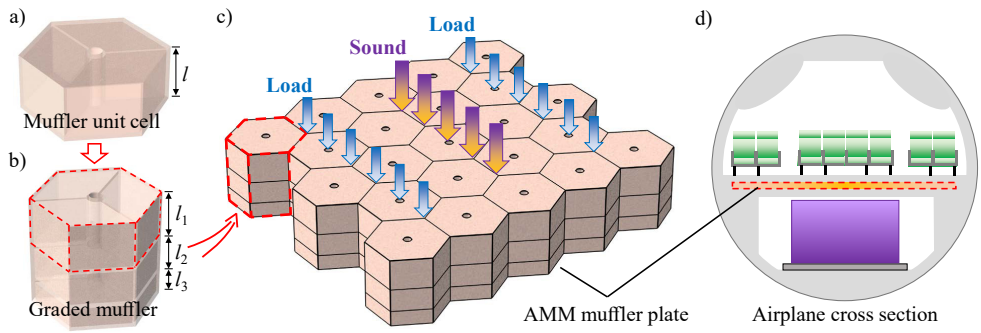

Fig. 1. Honeycomb based graded metamaterial muffler: a) the muffler unit cell of lattice constant l; b) a graded muffler consisting of three unit cells with different lattice constants; c) an AMM muffler plate consisting of multiple graded mufflers arranged periodically; d) potential application in aircraft.

2. Theoretical model of unit cell

As shown in Fig. 2, the unit cell can be considered to be composed of three reinforcing ribs and a perforated cylindrical tube on the basis of a honeycomb cell. The geometric parameters of one unit cell are represented schematically by the explosion view and cross section. Here, l represents the lattice constant, a represents the side length of the regular hexagon, r_1 is the tube inner radius, r_2 is the perforation radius, t represents the honeycomb cell-wall thickness, tube wall thickness, reinforcing rib thickness, and end cover thickness. In this paper, the acoustic impedance of all possible solid materials is much higher than that of air, so from the perspective of aeroacoustics, all solid material boundaries can be regarded as hard acoustic field boundaries.

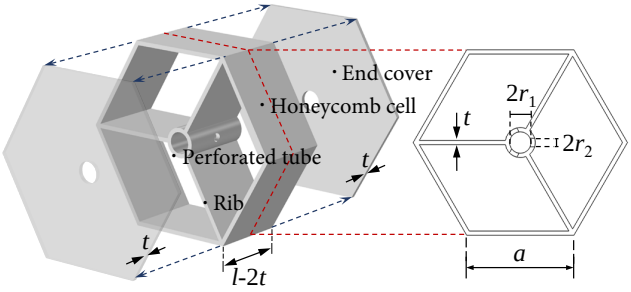

Fig. 2. Schematic illustration of the muffler unit cell with geometric parameters.

The unit cell contains three cavities, each of which works as an acoustic chamber resembling a Helmholtz resonator. When the resonator vibrates, it will radiate sound field to the surrounding medium, and the resonator will be affected by the field generated by itself. Consider a piston acoustic source of radius r_2 that vibrates at velocity $u = \overline{u}\exp(j\omega t)$, where $j = \sqrt{-1}$ is imaginary unit, ω is angular frequency, The additional radiation impedance (Junger, Feit, 1986) is given by:

$$Z_r = \rho_a c_a \pi r_2^2 \left[1 - \frac{J_1(2kr_2)}{kr_2} + j\frac{K_1(2kr_2)}{2(kr_2)^2}\right], \tag{1}$$

where J_1 is the Bessel function of first kind for order one, K_1 is the modified Bessel function of second kind for order one, k is wavenumber, ρ_a and c_a are the density and sound speed of air. When $kr_2 < 1$, the piston radiation reactance X_r can be obtained from the imaginary part of Z_r, that is, $X_r = \mathrm{Im}(Z_r) \approx 8\rho_a c_a k r_2^3/3$. Considering that the oscillator radiates in both positive and negative directions, the additional mass can be obtained as

$$M_r = \frac{2X_r}{\omega} = \frac{16}{3}\rho_a r_2^3. \tag{2}$$

Thus, the resonant frequency of Helmholtz resonator considering the additional mass correction caused by acoustic radiation can be written as:

$$f_H = \sqrt{\frac{\pi(r_2 c_a)^2}{4\pi^2 V_H\left[t + M_r/(\rho_a \pi r_2^2)\right]}}, \tag{3}$$

where

$$\begin{aligned} V_H &= (a^2/2 - \pi r_1^2/3)(l - 2t) \\ &\quad - \left(\sqrt{3}a - r_1 + 2\pi r_1/3\right)(l - 2t)t \\ &\quad + \left(1/2 - \sqrt{3}/6 - \pi/3\right)(l - 2t)t^2 \end{aligned}$$

is the acoustic chamber volume. To filter out acoustic waves at undesired frequencies, called target frequencies here, the design parameters should be adjusted so that the Helmholtz resonance frequency is equal to the target frequency.

Then consider the out-of-plane mechanics properties of the unit cell. Here the function of the honeycomb based unit cell is carrying normal loads in planes containing the axis of the hexagonal prism. The compressive moduli of the cell walls or ribs are much larger than the flexural moduli of the end covers. Thus, it is assumed that the carrying capacity of the end cover can be ignored. In addition, it is necessary to consider the negative effect of perforations on the bearing capacity of the cylindrical tube. An equivalent section method is adopted to simplify the part of the tube wall with a perforation to a wall of constant thickness, as shown in Fig. 3. The volume of the tube remains constant before and after the simplification, by which we can obtain the equivalent thickness

$$t_{eq} = \left[1 - \frac{2r_1 r_2^2}{l(2r_1 + t)\sqrt{r_1^2 - r_2^2}}\right]t, \tag{4}$$

and the equivalent cross sectional area of the unit cell

$$\begin{aligned} A_{eq} &= 3\pi(r_1 + t/2)\,t_{eq} + (9a - 3r_1 - \pi r_1)\,t \\ &\quad - \left(4\sqrt{3} + 3 + \pi/2\right)t^2. \end{aligned} \tag{5}$$

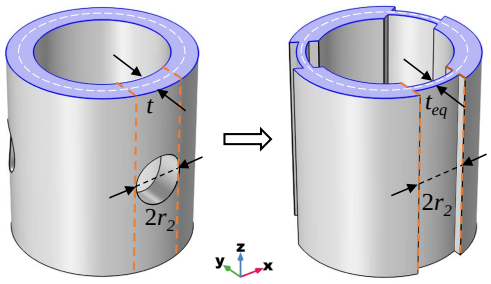

Fig. 3. Equivalent simplification of the perforated cylindrical tube.

It should be noted that the compressional wave velocity of the solid material c_s is equal to that of the unit cell c^*, that is

$$\sqrt{E_s/\rho_s} = \sqrt{E_c^*/\rho^*}, \tag{6}$$

where E_s and ρ_s are the Young's modulus and density of the solid material, respectively, E_c^* is the compressive modulus of the unit cell, and $\rho^* = m/(A^* l)$ is the density of the unit cell with $A^* = 3\sqrt{3}a^2/2$ being the area of the regular hexagon and m being the mass of the unit cell. Throughout, the subscript s refers to a property of the solid material while a superscripted * indicates an equivalent property of the unit cell itself. Accordingly, the compressive modulus of the unit cell is given by

$$E_c^* = \frac{E_s A_{eq}}{A^*}. \tag{7}$$

3. Finite element model

The range of acoustic band gap can be determined by the phonon dispersion curves, which, however, cannot reflect the attenuation degree of acoustic waves. Acoustic transmission loss (TL) can be used to demonstrate the effect of structure on acoustic wave attenuation at different frequencies. Phonon dispersion analysis and acoustic TL analysis can be conveniently introduced by taking the air domain inside the muffler structure as a unit cell either, here called an air unit cell to distinguish it from the original muffler unit cell. We assume small deformations here, and therefore neglect acoustoelastic coupling. FE models of the air unit cell (Fig. 4a) and muffler unit cell (Fig. 4b) are established to reveal acoustic and mechanical properties of unit cells with different lattice constants l through COMSOL Multiphysics. Bloch periodic boundary conditions (Bloch, 1929) are set on the two highlighted end faces in Fig. 4a for phonon dispersion analysis. When TL analysis is needed, the plane wave radiation boundary condition is set on one of the highlighted faces in Fig. 4a, and the perfect matching layer is set on the other face. Acoustic TL is defined as $\mathrm{TL} = 10\log(I_i/I_t)$, where I_i and I_t are the sound intensity of the incident wave and transmitted wave, respectively. To obtain the compression stiffness k^* and specific modulus E_c^*/ρ^* of the unit cell, a displacement w in the negative direction of z-axis is applied to the highlighted surface in Fig. 4b, and the z-axis displacement of the bottom surface is set to zero. The stiffness is calculated by $k^* = -f_c/w$. Then from the axial stress-strain relationship we can obtain the specific modulus $E_c^*/\rho^* = -f_c l/(\rho^* A^* w)$, where f_c is the constraining force on the bottom surface.

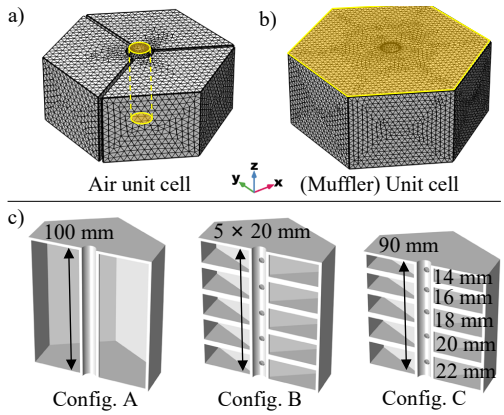

Fig. 4. a) Finite element model for the air domain (or air unit cell) enclosed by the muffler; b) a finite element model for the muffler unit cell; c) three different configurations of a honeycomb based muffler.

Three different configurations are designed to verify the performances of the honeycomb based unit cell and the superiority of graded muffler structure as shown in Fig. 4c. Configuration A is a common honeycomb cell with the reinforcing tube. Configuration B consists of five identical unit cells with the lattice constant of 20 mm. Configuration C is a graded metamaterial muffler with the total length of 90 mm, composed of five unit cells with graded changes in lattice constants. FE method (COMSOL Multiphysics) is used to calculate the TL and linear compression stiffness of the three configurations to compare their acoustic and mechanical properties.

4. Results and discussions

In this section, we first study the acoustic and mechanical properties of the muffler unit cell and then explore the influence of graded combination mode, namely, the offset ratio, on the performance of the muffler. Considering that the lattice constant corresponding to the target frequency is l, the offset ratio is defined as $\alpha = \Delta l/l$, where Δl is the deviation from the central lattice constant. Based on these studies, a graded muffler is designed and manufactured, and its sound insulation performance is tested by numerical methods. The improvement of sound insulation performance can be verified by comparing it with the other two configurations. In the following theoretical and numerical calculations, the physical parameters of air include: the density $\rho_a = 1.2\ \mathrm{kg/m^3}$, sound speed $c_a = 343.2\ \mathrm{m/s}$, dynamic viscosity $\eta_a = 1.84{\cdot}10^{-5}\ \mathrm{Pa\cdot s}$, bulk viscosity $\eta_B = 1.09\cdot 10^{-5}\ \mathrm{Pa\cdot s}$, ratio of specific heat $\gamma_a = 1.4$, specific heat capacity $C_a = 1000\ \mathrm{J/(kg\cdot K)}$, and thermal conductivity $\kappa_a = 0.026\ \mathrm{W/(m\cdot K)}$. The physical parameters of the solid material in the theoretical and numerical calculations include: the density $\rho_s = 2600\ \mathrm{kg/m^3}$, Young's modulus $E_s = 70$ GPa, and Poisson's ratio $\nu_s = 0.3$. As shown in Fig. 2, the geometric parameters of the unit cell include: the regular hexagon side length $a = 50$ mm, the cylindrical tube inner radius $r_1 = 5$ mm and perforation radius $r_2 = 2$ mm, the thickness $t = 2$ mm.

4.1. Acoustic band gap of the unit cell

As shown in Fig. 5a, the acoustic band gap of the unit cell is given by the upper and lower edges, the

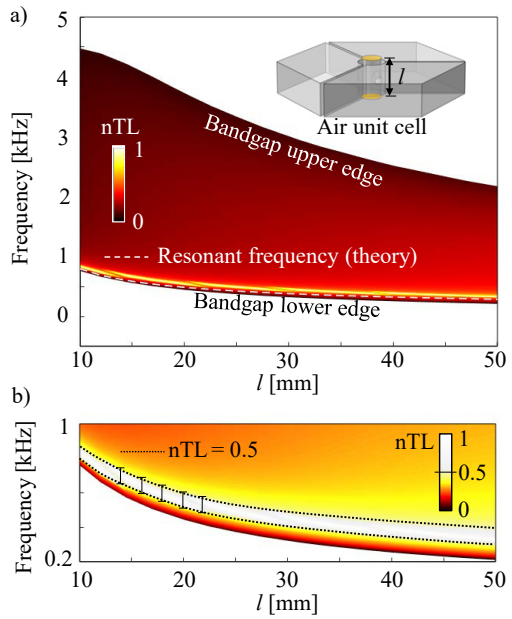

Fig. 5. a) Influences of the lattice constant on acoustic band gap frequency range and normalised transmission loss; b) a partial enlarged drawing of Fig. 5a.

detailed sound insulation capability at different frequencies within the band gap is denoted by the colour legend, and the white dashed line represents the Helmholtz resonance frequencies for different lattice constants calculated by theoretical model. Here, the normalised TL (nTL) is adopted because we are mainly concerned with the variation pattern of the peak frequency of sound insulation with respect to the lattice constant, rather than the absolute sound insulation. The maximum value of TL is set to 1 and the minimum value is set to 0. Overall, the theoretical and finite element model match well. It can be observed from Fig. 5a that the band gap beginning frequency is closely followed by the resonant frequency or target frequency. The unit cell has a wide acoustic band gap, but the nTL is not uniformly distributed in the band gap range. The sound insulation is significantly effective near the resonant frequency, as the incident wave frequency moves away from the resonant point, the normalised TL decreases sharply, as shown in Fig. 5b. These phenomena result from the local resonance mechanism (Liu *et al.*, 2005; Ding *et al.*, 2007; Zhou *et al.*, 2017), which can realise wave control by subwavelength structure but often leads to a strong but narrow attenuation band. As shown in Fig. 5b, compared with the gap bandwidth obtained by the dispersion curves, the actual sound insulation bandwidth considered to be effective (nTL ≥ 0.5) is very narrow. We can use the band gap range with strong sound insulation effect (nTL ≥ 0.5) to control the strong sound source of specific frequency, while the other band gap range is used for general frequency band insulation. Therefore, we consider combining unit cells with different lattice constants to form a graded structure for broadband sound attenuation. The band gap of nTL ≥ 0.5 is used as the design basis. It is noted that when the lattice constant l is smaller than 25 mm, the band gap frequency is more sensitive to the variation of the lattice constant.

4.2. Load bearing capability of the unit cell

The mechanical properties of unit cells with different lattice constants are shown in Fig. 6. The theory and the numerical results agree very well. The mechanical properties are described from two perspectives. The specific compression modulus (or specific modulus) characterises the equivalent properties of a muffler unit cell as a material, while the compression stiffness more directly reflects the ability of the unit cell as a structure to resist deformation. As the lattice constant increases, the specific modulus goes up, but the stiffness decreases, indicating an increase in relative efficiency against physical deformation, but a decrease in absolute resistance to deformation. Hence, the lattice constants should be selected according to practical needs in engineering applications.

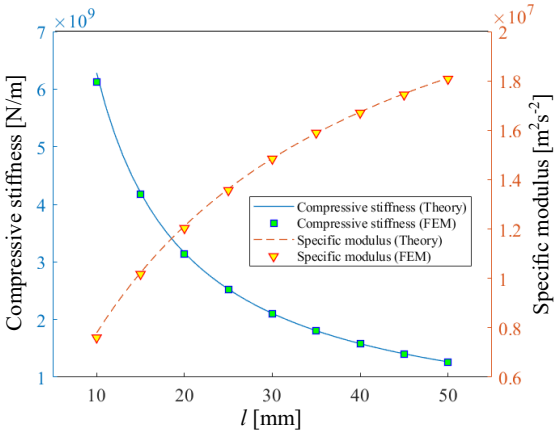

Fig. 6. Influences of the lattice constant on the unit cell compressive stiffness and specific modulus.

4.3. Influence of offset ratio

The influences of offset ratio α on the transmission loss and stiffness of graded structure are shown in Fig. 7. Considering that the lattice constant corresponding to the target frequency is l, the offset ratio is defined as $\alpha = \Delta l/l$, where Δl is the deviation from the central lattice constant. Here, a five-unit-cell graded structure is used to investigate the influence of offset ratio. The lattice constants of these five cells are $(1-2\alpha)l$, $(1-\alpha)l$, l, $(1+\alpha)l$, and $(1+2\alpha)l$. For $l = 20$ mm, the influence of the offset ratio on sound insulation is shown in Fig. 7a. It can be seen that as the offset ratio increases, the effective band gap width

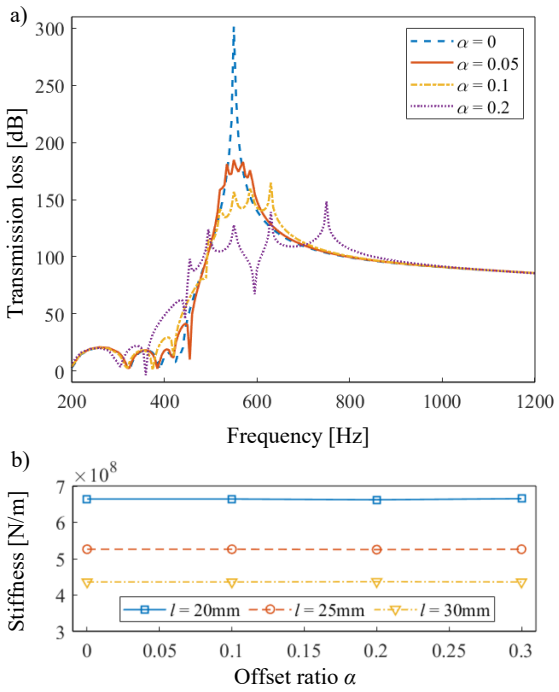

Fig. 7. Influence of the offset ratio on: a) transmission loss; b) compression stiffness under different lattice constants.

(nTL ≥ 0.5) becomes wider, but the attenuation magnitude of the peak transmission loss decreases. When the offset ratio is relatively small, such as 0.05, the peak is barely broadened. When the offset ratio is selected as a relatively large value, such as 0.2, the attenuation peak is divided into five separate parts, which is not expected to happen with band structures. Therefore, in order to achieve a wide and relatively high attenuation band gap, a medium α value, such as 0.1, is acceptable. The influence of the offset ratio on compression stiffness under different lattice constants is shown in Fig. 7b. It can be seen that the stiffness is negatively correlated with the lattice constant, but almost does not change with the offset ratio. This is because the horizontal cover plates are not the main components to bear axial compression, and the position of the covers has negligible effect on the stiffness, which brings more design flexibility.

4.4. Acoustic and mechanical properties of graded mufflers

As a result, five unit cells with lattice constants of 14 mm, 16 mm, 18 mm, 20 mm, and 22 mm are combined to construct a graded composite muffler (configuration C) for band gap broadening. The offset ratio of configuration C is 0.11, which is a moderate value, thus achieving a wide and relatively high attenuation gap. We compare the sound insulation characteristics of ordinary honeycomb cell (configuration A), uniform periodic muffler (configuration B), and graded composite muffler (configuration C), as shown in Fig. 8. Configuration A has no sound insulation peak due to the absence of acoustic chambers. Configuration B has only one sharp TL peak because of its single resonant frequency. Configuration C has five peaks resulting from five different acoustic chambers. Compared with configuration B, configuration C has a smaller TL peak value, but the effective band gap width (nTL ≥ 0.5) is 47% wider, and geometrically configuration C is only 90% the size of configuration B, which means it is lighter and takes up less space. This broadband attenuation effect is numerically confirmed.

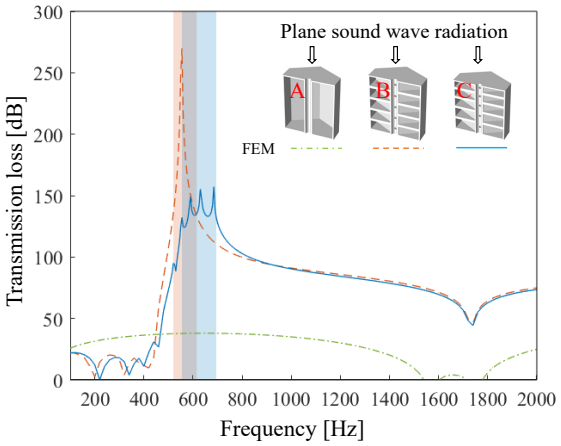

Fig. 8. Transmission loss of the three different muffler configurations.

To investigate the frequency dependent sound pressure distribution of the wave propagation path, its FE volume plots of sound pressure level (SPL) are presented in Fig. 9 at typical frequencies including 555 Hz (the TL peak frequency for both configuration B and configuration C) and 685 Hz (the TL peak frequency only for configuration C). The reference sound pressure is 20 μPa. It can be seen from Fig. 9 that the SPL in configuration B varies uniformly. At its TL peak frequency of 555 Hz (Fig. 9a), SPL drops evenly and rapidly along the sound propagation path. At 685 Hz (Fig. 9b), the SPL decreases relatively slowly, but still varies in a uniform way. For configuration C, when the incident wave frequency is equal to the resonant frequency of one of the acoustic cavities, a rapid drop of SPL occurs near this cavity, and this phenomenon is particularly obvious in Fig. 9d. At the acoustic cavity indicated by the arrow, the SPL drops by about 63 dB. It is the presence of multiple resonant frequencies that allows configuration C to have a broader band gap compared with configuration B, at the expense of part of the single frequency absorption capacity.

Through numerical simulation, the structural compressive stiffness of the three configurations A, B, and C (Fig. 4c) is obtained, which is $K_A = 4.62 \cdot 10^8$ N/m, $K_B = 6.64 \cdot 10^8$ N/m, and $K_C = 7.41 \cdot 10^8$ N/m, respectively. Configuration A (common honeycomb cell)

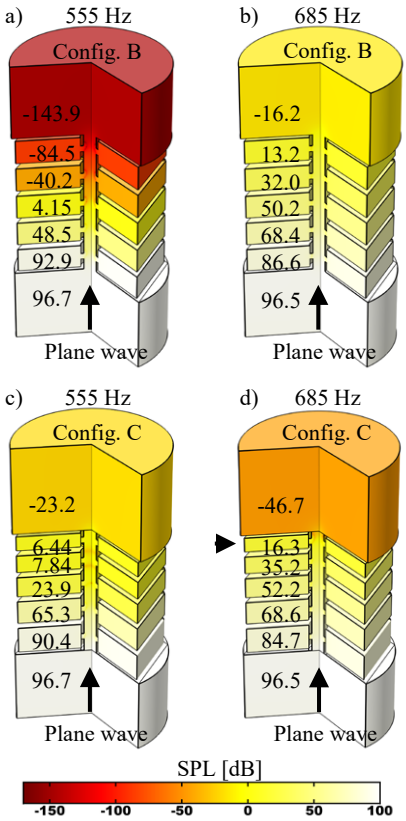

Fig. 9. Sound pressure level distributions of the two configurations of mufflers (configuration B and configuration C) at 555 Hz and 685 Hz.

has the worst stiffness characteristics. Configuration C (graded muffler) has 11.6% higher stiffness than that of configuration B (uniform periodic muffler) while its length is 10% shorter and the mass is 4.5% lighter. This is because shorter and lighter unit cells have greater stiffness, as shown in Fig. 7b. Due to the series arrangement of unit cells in configurations B and C, we can estimate the equivalent stiffness of the two structures by regarding them as multiple springs in series. That is, a single unit cell is regarded as a spring, and a combination of multiple cells is regarded as a series of springs. According to the stiffness of a unit cell obtained in Subsec. 4.2, $K_B = 6.31 \cdot 10^8$ N/m and $K_C = 7.12 \cdot 10^8$ N/m are calculated by the spring series formula, neither deviation from the numerical result is more than 5%.

5. Conclusion

The proposed honeycomb based graded metamaterial muffler shows excellent broadband sound attenuation and stiffness properties. Based on the Helmholtz resonance theory and cellular solids theory, acoustic and mechanical theoretical models are established, respectively. Also, different finite element models are developed via the commercial software COMSOL Multiphysics for comparison. The finite element calculation results match well with the theoretical results. The results show that acoustic metamaterials can be used as both structural and functional materials by setting up resonance structures in cellular solids. In addition, by introducing graded structure design, the effective subwavelength band gap can be extended at a certain offset ratio, at the cost of the loss of acceptable single frequency muffling effect. The graded muffler is superior to the uniform muffler in the noise elimination effect and stiffness characteristics. Therefore, the proposed metamaterial muffler achieves broadband sound attenuation without loss of bearing performance, which shows promising potential for noise control engineering.

Acknowledgments

The presented work is funded by National Natural Science Foundation of China (Grant No. 12072153).

References

1. Aboudi J., Pindera M.-J., Arnold S.M. (1999), Higher-order theory for functionally graded materials, *Composites Part B: Engineering*, **30**(8): 777–832, doi: 10.1016/S1359-8368(99)00053-0.
2. Asprone D., Auricchio F., Menna C., Morganti S., Prota A., Reali A. (2013), Statistical finite element analysis of the buckling behavior of honeycomb structures, *Composite Structures*, **105**: 240–255, doi: 10.1016/j.compstruct.2013.05.014.
3. Bloch F. (1929), About the quantum mechanics of electrons in crystal lattices [in German], *Zeitschrift für Physik*, **52**(7): 555–600, doi: 10.1007/BF01339455.
4. Brennan M.J. (1997), Characteristics of a wideband vibration neutralizer, *Noise Control Engineering Journal*, **45**(5): 201–207, doi: 10.3397/1.2828441.
5. Camata G., Shing P.B. (2010), Static and fatigue load performance of a GFRP honeycomb bridge deck, *Composites Part B: Engineering*, **41**(4): 299–307, doi: 10.1016/j.compositesb.2010.02.005.
6. Chen Q. *et al.* (2016), Plastic collapse of cylindrical shell-plate periodic honeycombs under uniaxial compression: experimental and numerical analyses, *International Journal of Mechanical Sciences*, **111–112**: 125–133, doi: 10.1016/j.ijmecsci.2016.03.020.
7. Chen W.Q., Lee K.Y. (2003), Alternative state space formulations for magnetoelectric thermoelasticity with transverse isotropy and the application to bending analysis of nonhomogeneous plates, *International Journal of Solids and Structures*, **40**(21): 5689–5705, doi: 10.1016/S0020-7683(03)00339-1.
8. Chen X., Xu X., Ai S., Chen H., Pei Y., Zhou X. (2014), Active acoustic metamaterials with tunable effective mass density by gradient magnetic fields, *Applied Physics Letters*, **105**(7): 071913, doi: 10.1063/1.4893921.

9. Chen Y., Chen G., Li G., He H. (2021a), Modal analysis of flexural band gaps in a membrane acoustic metamaterial (MAM) and waveguides affected by shape characteristics, *Physics Letters A*, **414**: 127635, doi: 10.1016/j.physleta.2021.127635.

10. Chen Y., Li G., Sun R., Chen G. (2021b), Wave dispersion in one-dimensional nonlinear local resonance phononic crystals with perturbation method, *Crystals*, **11**(7): 1–15, doi: 10.3390/cryst11070774.

11. Cheng Z.-Q. (2001), Nonlinear bending of inhomogeneous plates, *Engineering Structures*, **23**(10): 1359–1363, doi: 10.1016/S0141-0296(01)00017-7.

12. Correa D.M., Seepersad C.C., Haberman M.R. (2015), Mechanical design of negative stiffness honeycomb materials, *Integrating Materials and Manufacturing Innovation*, **4**(1): 165–175, doi: 10.1186/s40192-015-0038-8.

13. Deymier P.A. [Ed.] (2013), *Acoustic Metamaterials and Phononic Crystals*, Springer, doi: 10.1007/978-3-642-31232-8.

14. Ding Y., Liu Z., Qiu C., Shi J. (2007), Metamaterial with simultaneously negative bulk modulus and mass density, *Physical Review Letters*, **99**(9): 2–5, doi: 10.1103/PhysRevLett.99.093904.

15. Fan X., Verpoest I., Vandepitte D. (2006), Finite element analysis of out-of-plane compressive properties of thermoplastic honeycomb, *Journal of Sandwich Structures & Materials*, **8**(5): 437–458, doi: 10.1177/1099636206065862.

16. Han B., Wang W., Zhang Z., Zhang Q., Jin F., Lu T. (2016), Performance enhancement of sandwich panels with honeycomb–corrugation hybrid core, *Theoretical and Applied Mechanics Letters*, **6**(1): 54–59, doi: 10.1016/j.taml.2016.01.001.

17. Huang J., Gong X., Zhang Q., Scarpa F., Liu Y., Leng J. (2016), In-plane mechanics of a novel zero Poisson's ratio honeycomb core, *Composites Part B: Engineering*, **89**: 67–76, doi: 10.1016/j.compositesb.2015.11.032.

18. Jabbari M., Sohrabpour S. (2014), Mechanical and thermal stresses in a functionally graded hollow cylinder due to nonaxisymmetric steady-state loads, [in:] *Encyclopedia of Thermal Stresses,* Hetnarski R.B. [Ed.], pp. 2946–2952, Springer, Dordrecht, doi: 10.1007/978-94-007-2739-7_959.

19. Junger M.C., Feit D. (1986), *Sound, structures, and their interaction*, The MIT Press: Cambridge, Massachusetts, London, England.

20. Kawasaki A., Watanabe R. (1997), Concept and P/M fabrication of functionally gradient materials, *Ceramics International*, **23**(1): 73–83, doi: 10.1016/0272-8842(95)00143-3.

21. Khan M.K., Baig T., Mirza S. (2012), Experimental investigation of in-plane and out-of-plane crushing of aluminum honeycomb, *Materials Science and Engineering: A*, **539**: 135–142, doi: 10.1016/j.msea.2012.01.070.

22. Koizumi M. (1997), FGM activities in Japan, *Composites Part B: Engineering*, **28**(1–2): 1–4, doi: 10.1016/S1359-8368(96)00016-9.

23. Kushwaha M.S., Halevi P., Dobrzynski L., Djafari-Rouhani B. (1993), Acoustic band structure of periodic elastic composites, *Physical Review Letters*, **71**(13): 2022–2025, doi: 10.1103/PhysRevB.49.2313.

24. Li Z., Wang T., Jiang Y., Wang L., Liu D. (2018), Design-oriented crushing analysis of hexagonal honeycomb core under in-plane compression, *Composite Structures*, **187**: 429–438, doi: 10.1016/j.compstruct.2017.12.066.

25. Liu J., Wang Z., Hui D. (2018), Blast resistance and parametric study of sandwich structure consisting of honeycomb core filled with circular metallic tubes, *Composites Part B: Engineering*, **145**: 261–269, doi: 10.1016/j.compositesb.2018.03.005.

26. Liu Z. *et al.* (2000), Locally resonant sonic materials, *Science*, **289**(5485): 1734–1736, doi: 10.1126/science.289.5485.1734.

27. Liu Z., Chan C.T., Sheng P. (2005), Analytic model of phononic crystals with local resonances, *Physical Review B – Condensed Matter and Materials Physics*, **71**(1): 1–8, doi: 10.1103/PhysRevB.71.014103.

28. Martínez-Sala R., Sancho J., Sánchez J.V., Gómez V., Llinares J., Meseguer F. (1995), Sound attenuation by sculpture, *Nature*, **378**(6554): 241, doi: 10.1038/378241a0.

29. Michailidis P.A., Triantafyllidis N., Shaw J.A., Grummon D.S. (2009), Superelasticity and stability of a shape memory alloy hexagonal honeycomb under in-plane compression, *International Journal of Solids and Structures*, **46**(13): 2724–2738, doi: 10.1016/j.ijsolstr.2009.03.013.

30. Montero de Espinosa F.R., Jiménez E., Torres M. (1998), Ultrasonic Band Gap in a Periodic Two-Dimensional Composite, *Physical Review Letters*, **80**(6–9): 1208–1211, doi: 10.1103/PhysRevLett.80.1208.

31. Naebe M., Shirvanimoghaddam K. (2016), Functionally graded materials: A review of fabrication and properties, *Applied Materials Today*, **5**: 223–245, doi: 10.1016/j.apmt.2016.10.001.

32. Narayanamurti V., Strömer H.L., Chin M.A., Gossard A.C., Wiegmann W. (1979), Selective transmission of high-frequency phonons by a superlattice: the "dielectric" phonon filter, *Physical Review Letters*, **43**(27): 2012–2016, doi: 10.1103/PhysRevLett.43.2012.

33. Nishida E., Koopmann G.H. (2007), A method for designing and fabricating broadband vibration absorbers for structural noise control, *Journal of Vibration and Acoustics, Transactions of the ASME*, **129**(4): 397–405, doi: 10.1115/1.2424968.

34. Popa B.I., Zigoneanu L., Cummer S.A. (2013), Tunable active acoustic metamaterials, *Physical Review B – Condensed Matter and Materials Physics*, **88**(2): 1–8, doi: 10.1103/PhysRevB.88.024303.

35. Qian D., Shi Z. (2017), Using PWE/FE method to calculate the band structures of the semi-infinite PCs: periodic in x-y plane and finite in z–direction, *Archives of Acoustics*, **42**(4): 735–742, doi: 10.1515/aoa-2017-0076.

36. Shao H., He H., Chen G., Chen Y. (2020), Two new designs of lamp-type piezoelectric metamaterials for active wave propagation control, *Chinese Journal of Physics*, **65**: 1–13, doi: 10.1016/j.cjph.2020.02.015.

37. Shen H.-S. (2002), Postbuckling analysis of axially loaded functionally graded cylindrical panels in thermal environments, *International Journal of Solids and Structures*, **39**(24): 5991–6010, doi: 10.1016/S0020-7683(02)00479-1.

38. Sigalas M.M., Economou E.N. (1992), Elastic and acoustic wave band structure, *Journal of Sound and Vibration*, **158**(2): 377–382, doi: 10.1016/0022-460X(92)90059-7.

39. Sun G., Hou X., Chen D., Li Q. (2017), Experimental and numerical study on honeycomb sandwich panels under bending and in-panel compression, *Materials & Design*, **133**: 154–168, doi: 10.1016/j.matdes.2017.07.057.

40. Tsukamoto H. (2003), Analytical method of inelastic thermal stresses in a functionally graded material plate by a combination of micro- and macromechanical approaches, *Composites Part B: Engineering*, **34**(6): 561–568, doi: 10.1016/S1359-8368(02)00037-9.

41. Vasseur J.O., Deymier P.A., Frantziskonis G., Hong G., Djafari-Rouhani B., Dobrzynski L. (1998), Experimental evidence for the existence of absolute acoustic band gaps in two-dimensional periodic composite media, *Journal of Physics: Condensed Matter*, **10**(27): 6051–6064, doi: 10.1088/0953-8984/10/27/006.

42. Wang G., Chen S. (2015), Large low-frequency vibration attenuation induced by arrays of piezoelectric patches shunted with amplifier–resonator feedback circuits, *Smart Materials and Structures*, **25**(1): 15004, doi: 10.1088/0964-1726/25/1/015004.

43. Wang G., Wang J., Chen S., Wen J. (2011), Vibration attenuations induced by periodic arrays of piezoelectric patches connected by enhanced resonant shunting circuits, *Smart Materials and Structures*, **20**(12): 125019, doi: 10.1088/0964-1726/20/12/125019.

44. Wang T., An J., He H., Wen X., Xi X. (2021), A novel 3D impact energy absorption structure with negative Poisson's ratio and its application in aircraft crashworthiness, *Composite Structures*, **262**: 113663, doi: 10.1016/j.compstruct.2021.113663.

45. Wang Z. (2019), Recent advances in novel metallic honeycomb structure, *Composites Part B: Engineering*, **166**: 731–741, doi: 10.1016/j.compositesb.2019.02.011.

46. Wang Z., Liu J. (2018), Mechanical performance of honeycomb filled with circular CFRP tubes, *Composites Part B: Engineering*, **135**: 232–241, doi: 10.1016/j.compositesb.2017.09.048.

47. Wang Z., Liu J. (2019), Numerical and theoretical analysis of honeycomb structure filled with circular aluminum tubes subjected to axial compression, *Composites Part B: Engineering*, **165**: 626–635, doi: 10.1016/j.compositesb.2019.01.070.

48. Xiang J., Du J. (2017), Energy absorption characteristics of bio-inspired honeycomb structure under axial impact loading, *Materials Science and Engineering: A*, **696**: 283–289, doi: 10.1016/j.msea.2017.04.044.

49. Xiao S., Ma G., Li Y., Yang Z., Sheng P. (2015), Active control of membrane-type acoustic metamaterial by electric field, *Applied Physics Letters*, **106**(9), doi: 10.1063/1.4913999.

50. Zarei Mahmoudabadi M., Sadighi M. (2011), A study on the static and dynamic loading of the foam filled metal hexagonal honeycomb – Theoretical and experimental, *Materials Science and Engineering: A*, **530**: 333–343, doi: 10.1016/j.msea.2011.09.093.

51. Zhou J., Wang K., Xu D., Ouyang H. (2017), Multi-low-frequency flexural wave attenuation in Euler–Bernoulli beams using local resonators containing negative-stiffness mechanisms, *Physics Letters A*, **381**(37): 3141–3148, doi: 10.1016/j.physleta.2017.08.020.